Measurement of the Cosmic Ray Composition at the Knee with the SPASE-2/AMANDA-B10 Detectors

K. Rawlins[1], for the SPASE[2] and AMANDA[3] Collaborations
(1) Dept. of Physics, University of Wisconsin, Madison, WI 53706
(2) See J.E. Dickinson et al. (reference [1] in this paper) for author list
(3) See G.C. Hill et al. (in these proceedings) for author list

Abstract

Measuring the mass composition of cosmic rays at energies above 10^{15}eV, the region of the "knee", can provide crucial information for the understanding of the origin of cosmic rays. The SPASE-2 surface air shower array and the AMANDA-B10 neutrino telescope at the South Pole are used in coincidence to measure air showers at these energies. Information from the electron component at SPASE and the high-energy muon component at AMANDA are used together to determine the change of the cosmic ray mass composition in the energy range from 400 TeV to 6 PeV. Mass composition was calibrated to existing data from direct measurements at low energies. Our data show an increase of the mean log atomic mass $\langle \ln A \rangle$ within the energy range studied. We also discus the robustness of this technique against various systematic effects.

SPASE and AMANDA: Detectors and Reconstruction

Multicomponent measurements are needed to obtain primary energy and mass from an air shower. The South Pole Air Shower Experiment (SPASE-2) [1] reconstructs the shower direction from the arrival times in its scintillators. This track is required to pass within AMANDA's geometric volume, otherwise the event is discarded. The shower core position and shower size are reconstructed by fitting the lateral distribution of particle density to the Nishimura-Kamata-Greisen (NKG) function [2] and then evaluating the fit at a fixed distance (30 m) from the shower core. The density of charged particles is measured by this parameter, $S(30)$. Showers with an $S(30)$ less than 5 m^{-2} or with a core located outside the SPASE array are discarded.

The high-energy (> 300 GeV) muon component of the shower can penetrate to AMANDA depth as a muon bundle. Reconstruction of a coincidence event in AMANDA [3] requires two steps. First, the combined detectors (separated by 1750 m center-to-center) are used to get the bundle's position and direction, by fixing the track position at the shower core in SPASE and reconstructing the direction with AMANDA, allowing only the angles (θ, ϕ) to vary. Second, the

pp. 173–176

expected lateral distribution function (LDF) of photons from a muon bundle is computed, corrected for both the range-out of muons between the top of the detector and the bottom, and the changing scattering length as a function of depth in the ice, due to dust layers. A YAG laser at a wavelength of 532 nm was used to map the scattering and absorption lengths as a function of depth [4]. With the track position and direction held fixed, the OM amplitudes in the event are fit to this functional form. The overall normalization and the bulk propagation length (λ_0) are left as free parameters. Distributions of each agree well in data and Monte Carlo; outlier events with an unphysical λ_0 are discarded. The parameter $K50$ is then defined as the fit LDF evaluated at a perpendicular distance of 50 m at a nominal position along the trajectory. 50 m offers the most stable measurement under simultaneous variations of fitted parameters [5]. $K50$, which has units of photoelectrons/OM, is a composition-independent measurement of the total muon energy, as shown by simulations in Figure 1.

Primary Energy and Composition Analysis

The two observables $\log K50$ and $\log S(30)$ form a 2-dimensional parameter space shown in Figure 2, in which primary energy and primary mass separate, and each event can be identified with a reconstructed energy and mass. For a given primary energy, iron-induced showers are more muon-rich and develop higher in the atmosphere than proton-induced showers. Thus $K50$ is enhanced relative to $S(30)$ for heavy primaries, as one can see in Figure 2. Events at constant energy lie on an axis rotated by 24° in $\log S(30)$-$\log K50$ space; a set of axes rotated by this amount defines estimators of energy and mass on an event-by-event basis.

The Monte Carlo simulations indicate a mass independent energy resolution of $\sigma \simeq 0.1$ in $\log(E)$ at energies near 100 TeV, improving to 0.07 in the region of the knee and 0.06 at 30 PeV. The combined detector's response is linear up to about 10 PeV. The formal procedure for measuring mass composition takes place in six energy bins, shown in Figure 2. In each bin, the reconstructed mass distribution is compared to a series of mixtures of Monte Carlo proton and iron showers, each corresponding to a different mean log mass $\langle \ln A \rangle$. The technique is illustrated in Figure 3 for a sample energy bin.

The technique is calibrated at low energies using a vertical slice of events from $S(30) = 5 \rightarrow 10$ (see Figure 2), which corresponds to 200-350 TeV protons and about twice this energy for iron. Monte Carlo events, which are generated over a wide energy range using the same spectral index for each component, are weighted by a relative proportion which represents a mixed composition, or $\langle \ln A \rangle$. This mean log mass at fixed energy is taken from direct measurements such as RUNJOB [6] to be $\langle \ln A \rangle \approx 2.0$. A constant offset in $\log_{10}(K50)$ is found which makes the data and Monte Carlo reconstructed $K50$ distributions agree best in the $S(30)$ slice. Results using different initial calibration masses are used

to estimate the systematic error due to uncertainties in the direct measurement.

Choices of hadronic interaction, muon propagation, and detector models each correspond to a different absolute normalization for the $K50$ parameter. However, calibrating data to Monte Carlo at low energies in this way is a technique adaptable to any model, hence alternative models can help gauge the stability of this technique under model variation. The baseline Monte Carlo simulations [7] employ the air shower code MOCCA [8] using the QGSJET98 interaction model, a SPASE detector simulation, the muon propagator PROPMU [9], and a detailed AMANDA detector simulation. The explored alternatives include: an ice model without dust layers, a 4-component (p, He, O, Fe) model, SIBYLL for hadronic interaction, MMC [10] for muon propagation, and an electronics configuration which results in a loss of photon counting accuracy. Each alternative model is calibrated and analyzed independently using the technique described above.

Results and Conclusions

Results using SPASE/AMANDA coincidence data from 1998 are shown in Figure 4. Variation in results due to alternative models and changing low-energy calibration mass are also shown. The data are consistent with an unchanging mass compoition of $\langle \ln A \rangle = 2.0$ between 500 TeV and 1.2 PeV. The mass rises to $\langle \ln A \rangle = 2.9$ at 6 PeV, although the size of the error bars in these last bins allows our data to be consistent with a range of masses. While there are systematic shifts in the *absolute* $\langle \ln A \rangle$ between different models, all of the composition results follow a similar trend.

AMANDA measures the light output from the entire muon bundle over a track length of 500 m and laterally out to 150 m. Yet, the energy threshold is low enough to overlap with direct measurements for calibration. Because of the constant distance at which $K50$ is evaluated, different models are probed only for the difference between proton- and iron-induced showers and their energies. Thus, the method of probing the relative change of the ratio of muon energy to electromagnetic energy in the air shower is robust and model independent.

1. J.E. Dickinson *et al.*, *Nucl. Instr. and Meth. A* **440** (2000) 95.
2. K. Greisen, *Progress in Cosmic Ray Physics* **3** (1956) 1.
3. J. Ahrens *et al.*, *Phys. Rev. D* **66** (2002) 012005.
4. K. Woschnagg *et al.*, *Proc. of 26th ICRC (Salt Lake City)* **2** (1999) 200.
5. K. Rawlins, Ph.D. Dissertation, UW-Madison (2001)
6. A.V. Apanasenko *et al.*, *Proc. of 27th ICRC (Hamburg)* (2001) 1622.
7. R. Engel, private communication..
8. A.M. Hillas, *Proc. 24th ICRC. (Rome)* **1** (1995) 270.
9. P. Lipari and T. Stanev, *Phys. Rev. D* **44** (1991) 3543.
10. W. Rhode and D. Chirkin *et al. Proc. of 27th ICRC (Hamburg)* (2001) 1017.

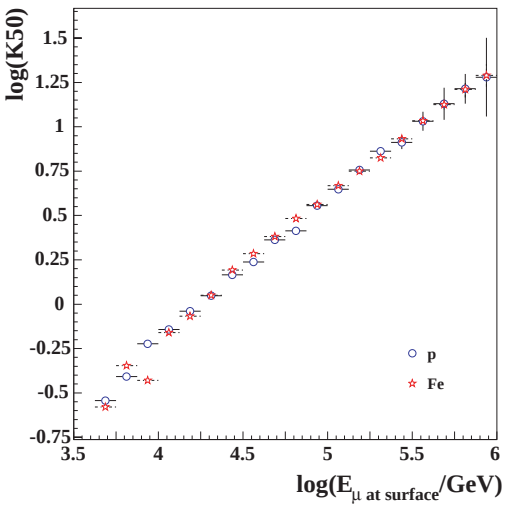

Fig. 1. $K50$ vs. the true total muon energy at the surface, for simulated proton and iron events.

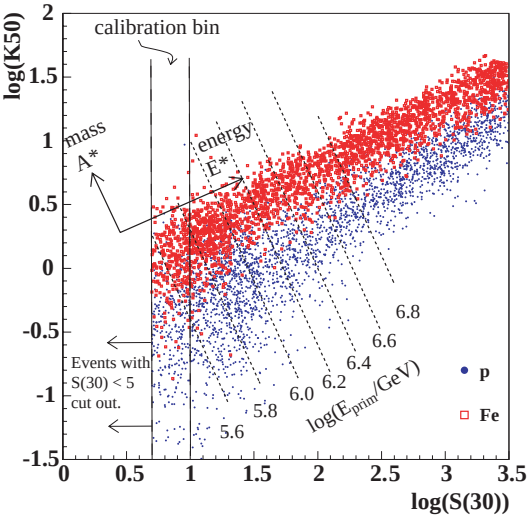

Fig. 2. $K50$ vs. $S(30)$ for simulated proton and iron events. The slice used for calibration, and the energy bins used for the final composition analysis, are also shown.

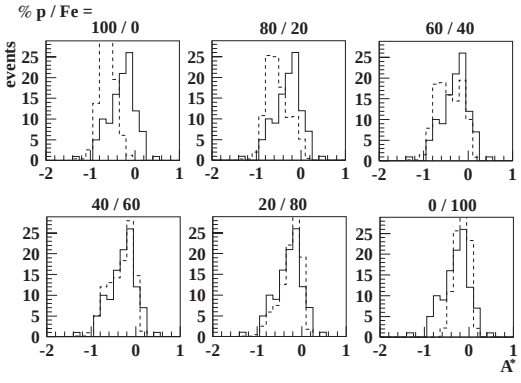

Fig. 3. Sample composition mixtures of p- and Fe-induced showers (dashed), and how they can be compared to data (solid). The *best* mixture is found by scanning through possible mixtures and measuring the probability that the data matches each hypothesis mixture using a maximum-likelihood method.

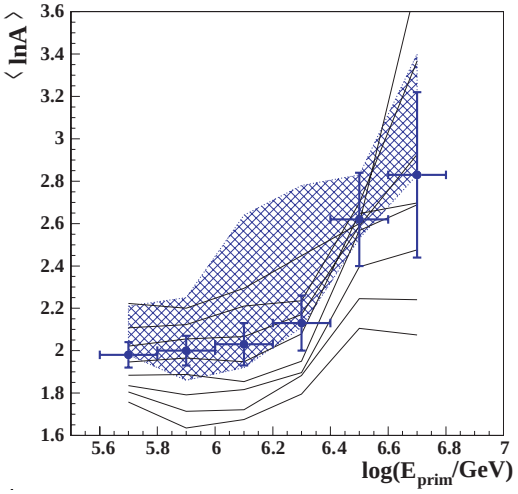

Fig. 4. The mean log mass as a function of primary energy. Circular points indicate the results from the baseline model, with one standard deviation statistical error bars. The shaded band indicates the range of results obtained using alternative simulations. The solid lines indicate results using different initial calibration masses at low energy.